Title

Association of Baseline Luminal Narrowing With Ileal Microbial Shifts and Gene Expression Programs and Subsequent Transmural Healing in Pediatric Crohn Disease

Journal

Inflammatory Bowel Diseases, 27(11)

ISSN

1078-0998

Authors

Ta, Allison D
Ollberding, Nicholas J
Karns, Rebekah
et al.

Publication Date

2021-10-20

DOI

10.1093/ibd/izaa339

Peer reviewed

Inflammatory Bowel Diseases, 2021, **27**, 1707–1718
DOI: 10.1093/ibd/izaa339
Advance access publication 16 January 2021
Leading Off

Association of Baseline Luminal Narrowing With Ileal Microbial Shifts and Gene Expression Programs and Subsequent Transmural Healing in Pediatric Crohn Disease

Allison D Ta, MD,[*] Nicholas J Ollberding, PhD,[*] Rebekah Karns, PhD,[*] Yael Haberman, MD, PhD,[*,†] Adina L Alazraki, MD,[‡] David Hercules,[‡] Robert Baldassano, MD,[§] James Markowitz, MD,[¶] Melvin B Heyman, MD,[‖] Sandra Kim, MD,[**] Barbara Kirschner, MD,[††] Jason M Shapiro, MD,[‡‡] Joshua Noe, MD,[§§] Maria Oliva-Hemker, MD,[¶¶] Anthony Otley, MD,[‖‖] Marian Pfefferkorn, MD,[***] Richard Kellermayer, MD,[†††] Scott Snapper, MD,[‡‡‡] Shervin Rabizadeh, MD,[§§§] Ramnik Xavier, MD, PhD,[¶¶¶,‖‖‖] Marla Dubinsky, MD,[****] Jeffrey Hyams, MD,[††††] Subra Kugathasan, MD,[‡] Anil G Jegga, DVM, MS,[*] Jonathan R Dillman, MD, MSc,[*] and Lee A Denson, MD[*]

From the *Cincinnati Children's Medical Hospital Center and the University of Cincinnati College of Medicine, Cincinnati, Ohio, USA
[†]Sheba Medical Center, Tel-HaShomer, affiliated with the Tel-Aviv University, Tel Aviv, Israel
[‡]Emory University and Children's Healthcare of Atlanta, Atlanta, Georgia, USA
[§]The Children's Hospital of Philadelphia, Philadelphia, Pennsylvania, USA
[¶]Cohen Children's Medical Center of New York, New Hyde Park, New York, USA
[‖]University of California San Francisco, San Francisco, California, USA
[**]Children's Hospital of Pittsburgh of UPMC, Pittsburgh, Pennsylvania, USA
[††]The University of Chicago, Chicago, Illinois, USA
[‡‡]Hasbro Children's Hospital, Providence, Rhode Island, USA
[§§]Medical College of Wisconsin, Milwaukee, Wisconsin, USA
[¶¶]John Hopkins University, Baltimore, Maryland, USA
[‖‖]IWK Health Centre, Halifax, Nova Scotia, Canada
[***]Indiana University School of Medicine, Indianapolis, Indiana, USA
[†††]Texas Children's Hospital, Baylor College School of Medicine, Houston, Texas, USA
[‡‡‡]Children's Hospital-Boston, Boston, Massachusetts, USA
[§§§]Cedars-Sinai Medical Center, Los Angeles, California, USA
[¶¶¶]Broad Institute at Massachusetts Institute of Technology, Cambridge, Massachusetts, USA
[‖‖‖]Massachusetts General Hospital, Cambridge, Massachusetts, USA
[****]Mount Sinai Hospital, New York, New York, USA
[††††]Connecticut Children's Medical Center, Hartford, Connecticut, USA

Address correspondence to: Lee A. Denson, MD, 3333 Burnett Avenue, MLC 2010, Cincinnati, OH 45229 (lee.denson@cchmc.org).

Background: Transmural healing (TH) is associated with better long-term outcomes in Crohn disease (CD), whereas pretreatment ileal gene signatures encoding myeloid inflammatory responses and extracellular matrix production are associated with stricturing. We aimed to develop a predictive model for ileal TH and to identify ileal genes and microbes associated with baseline luminal narrowing (LN), a precursor to strictures.

Materials and Methods: Baseline small bowel imaging obtained in the RISK pediatric CD cohort study was graded for LN. Ileal gene expression was determined by RNASeq, and the ileal microbial community composition was characterized using 16S rRNA amplicon sequencing. Clinical, demographic, radiologic, and genomic variables were tested for association with baseline LN and future TH.

Results: After controlling for ileal location, baseline ileal LN (odds ratio [OR], 0.3; 95% confidence interval [CI], 0.1-0.8), increasing serum albumin (OR, 4; 95% CI, 1.3-12.3), and anti-*Saccharomyces cerevisiae* antibodies IgG serology (OR, 0.97; 95% CI, 0.95-1) were associated with subsequent TH. A multivariable regression model including these factors had excellent discriminant power for TH (area under the curve, 0.86; positive predictive value, 80%; negative predictive value, 87%). Patients with baseline LN exhibited increased Enterobacteriaceae and inflammatory and extracellular matrix gene signatures, coupled with reduced levels of butyrate-producing commensals and a respiratory electron transport gene signature. Taxa including Lachnospiraceae and the genus *Roseburia* were associated with increased respiratory and decreased inflammatory gene signatures, and *Aggregatibacter* and *Blautia* bacteria were associated with reduced extracellular matrix gene expression.

Conclusions: Pediatric patients with CD with LN at diagnosis are less likely to achieve TH. The association between specific microbiota, wound healing gene programs, and LN may suggest future therapeutic targets.

Key Words: microbiome, gene expression, luminal narrowing, magnetic resonance enterography, transmural healing

Received for publications: August 31, 2020.

Introduction

The incidence of pediatric Crohn disease (CD) has continued to rise over the past 3 decades.[1, 2] Recurrent episodes of active and chronic inflammation lead to the development of fibrosis creating intestinal luminal narrowing (LN), which can progress to a stricture, frequently requiring surgical resection. There remains a 25% lifetime risk of stricturing disease despite anti-tumor necrosis factor (TNF) therapy, which is of especially concern for the growing pediatric CD population.[3-5]

The RISK prospective multicenter inception cohort study evaluated pediatric patients with CD for the development of complications.[6] This study showed that up to 6% of pediatric patients with initial inflammatory behavior progress to isolated strictures by 36 months after diagnosis. Recently published American Gastroenterology Association (AGA)-Society of Abdominal Radiology (SAR) diagnostic imaging consensus guidelines[7] now classify the small bowel in patients with CD as having 1 of 4 possible radiologic (computed tomography and magnetic resonance enterography) appearances: (1) normal, (2) inflamed but without LN, (3) LN without prestenotic dilatation, and (4) stricture with persistent LN and prestenotic dilation ≥3 cm. This classification system provides a standardized approach for evaluating small bowel CD and differentiating LN as a precursor to stricture formation.

The primary therapeutic target for CD has been mucosal healing because of the association with long-term clinical remission and reduced surgical outcomes. However, mucosal healing does not address small bowel inflammation inaccessible by endoscopy or evaluate the deep tissue layers of the bowel that are involved in the development of stricturing disease. Recent studies have shown that transmural healing (TH), defined by imaging of the small bowel with deep transmural layer healing, has improved outcomes when compared to mucosal healing alone.[8-10]

A combination of gene expression pathways, immune dysregulation, and altered intestinal microbiota have been linked to the development of CD and stricture complications. Murine models and patient-based studies have shown that microbial shifts are associated with disease activity and the development of fibrosis.[11, 12] Proposed mechanisms related to the microbiota include host cellular alterations in gene expression, which promote extracellular matrix deposition and fibrosis. These findings have been supported by early upregulation of inflammatory and extracellular matrix gene expression in patients who develop fibrosis.[6, 13] These patients had enrichment of gene expression for extracellular matrix and inflammatory pathways that was associated with the activation of myofibroblasts, which are key to the development of fibrosis.

In this study, we developed a predictive multivariable model for achieving TH in a subgroup of patients from the pediatric RISK study based on a centralized reanalysis of the study's radiologic imaging conducted according to these recent AGA-SAR guidelines. Pretreatment ileal tissue samples underwent 16S rRNA gene sequencing for microbiotal taxonomic classification and RNASeq analysis for gene expression profiling. We utilized the CD imaging classification to identify novel relationships with gene expression and microbial taxa.

MATERIALS AND METHODS

RISK Clinical Cohort

The RISK cohort study enrolled 1136 children with CD at diagnosis at 28 sites across the United States and Canada from 2008 to 2012 (ClinicalTrials.gov identifier: NCT00790543).[6] Upon diagnosis with CD, patients were enrolled, clinical baseline data and biospecimens were collected, and follow-up was performed every 6 months over a 5-year period to assess for disease progression (data locked on May 3, 2020). Data included patient demographics, clinical history, and baseline antimicrobial serologies. Patients were required to undergo an endoscopic evaluation at diagnosis before treatment to confirm characteristics of ileitis/colitis by histology. The Montreal classification was used for disease location.[14] Patients were managed based on their primary physician's recommendations. For this current study, patients were divided into subgroups for each analysis based on available ileal pretreatment tissue for microbial 16S sequencing, high-quality ileal RNA for sequencing, and/or small bowel imaging (Supplemental Fig. 1).

Serologic Assays

Baseline blood samples were obtained for serologic determination[6, 15] of antimicrobial serology of the anti-*Saccharomyces cerevisiae* antibodies (ASCA) IgG, ASCA IgA, and anti-CBir1 at the Cedars-Sinai Hospital (Los Angeles, CA).[16] Serology levels were expressed as enzyme-linked immunosorbent assay units (EU/mL). Antibody results were compared to a Cedars-Sinai laboratory standard derived from a CD population with well-characterized disease and pooled patient sera with this antigen reactivity. The ASCA IgG was considered positive when >40 EU/mL, ASCA IgA was positive when >20 EU/mL, and anti-CBir1 was positive when >25 EU/mL.

Diagnostic Imaging Analysis

All relevant imaging examinations were reviewed by a board-certified, fellowship-trained pediatric radiologist with 10 years postfellowship experience. Cross-sectional imaging (including small bowel follow-through; n = 25), computed tomography (n = 20), computed tomography enterography (n = 23), and magnetic resonance enterography (n = 198) were analyzed using the 2018 AGA-SAR consensus guidelines for the presence of LN or stricture.[7] Baseline imaging was defined as images obtained at least 6 months after diagnosis. Follow-up imaging was any imaging obtained 6 months after diagnosis. Baseline and follow-up ileal imaging were classified for CD involvement as follows: (1) normal, (2) inflammation present (wall thickening and abnormal postcontrast hyperenhancement at computed tomography, computed tomography enterography, and magnetic resonance enterography) without LN, (3) inflammation with LN (reduction in the ileal lumen to ≤50% without upstream small bowel luminal dilation, and (4) stricture defined as LN with ≥3 cm prestenotic bowel dilation.[7] We defined TH as the resolution of bowel wall thickening, postcontrast hyperenhancement, and resolution of LN and any upstream dilation. As part of an ongoing consensus process for imaging classification, a second radiologist reviewed 33 baseline and 38 follow-up studies. There was agreement on all except 3 studies.

Microbial 16S Amplicon Sequencing and Analysis

Ileal DNA was isolated from pretreatment tissue samples and subjected to 16S rRNA gene sequencing with details for the protocols described previously.[17] Publicly available sequence files were retrieved from the National Center for Biotechnology Information Sequence Read Archive using the SRAToolKit (version 2.9.3). Paired-end fastq files were processed into zero radius operational taxonomic units (zOTUs) using the USEARCH (version 11.0.667) UNOISE3 algorithm.[18] Paired-end reads were merged using the fastq_mergepairs command, allowing for a maximum of 10 differences in the overlapping region and a merged read length of 240 to 270 bp. Sequences with no more than 1 expected error were retained as the seeds to form zOTUs and were dereplicated. Error-correction and chimera removal were performed via the unoise3 command with default settings. Reads were mapped to zOTUs using the USEARCH otutab command with default settings. Taxonomic classification was performed using the naive Bayesian classifier in QIIME2 (version 2019.7)[19] against the SILVA 13.8 reference database trimmed to the v4 region. Corrected sequences were inserted into the SILVA 13.8 phylogenic tree using the fragment insertion via the SATé-enabled phylogenetic placement technique[20] as implemented in QIIME2. The zOTU table, taxonomy, representative sequences, phylogenetic tree, and clinical metadata were integrated into a single phyloseq object[21] for downstream statistical analyses. Sequence data obtained from terminal ileum samples and those with at least 3k reads after error correction were retained for analysis. Observed zOTUs and Shannon diversity were calculated using phyloseq (version 1.28.0) after subsampling to the lowest observed read depth >3k reads. Ordinary least-squares regression was used to test for differences in alpha-diversity estimates. Principal components analysis was conducted on the raw counts after variance-stabilizing transformation as implemented in DESeq2 (version 1.24.0).[22] Moderated negative binomial regression as implemented by DESeq2 was used to estimate log2 fold-changes and identify differentially abundant zOTUs for prevalent sequence variants detected in at least 20% of the samples.

RNA Sequencing and Analysis

Ileal RNA was isolated from pretreatment ileal biopsies as previously described.[6, 23] RNAseq libraries were determined using the NEBNext Ultra RNA Library Prep Kit (NEB, Ipswich, MA). The libraries used paired-end 150 base pair chemistry on the HiSeq system (GENEWIZ, South Plainfield, NJ). Kallisto[24] was used to quantify reads (coverage with median of 35.4M; interquartile ratio, 32.2M-39.4M) with transcripts per million as an output, and the reference genome was Gencode v24. Data included 14,370 protein-coding genes with transcripts per million > 1 in 20% of samples. Differentially expressed genes between CD with LN at baseline vs CD without LN at baseline with fold change differences ≥1.5 and using false discovery rate correction (≤0.05) were determined using R package DESeq2 version 1.24.0 and importing and summarizing the Kallisto output files to gene level with R package tximport version 1.12.3. Gene expression by RNASeq for the respiratory, inflammatory, and extracellular matrix gene panels was reduced to principal component 1 (PC1) for each participant (Supplemental Table 1). Functional annotation enrichment analyses were performed using the ToppGene Suite[25] and ToppCluster[26] web servers. For each gene list, we evaluated the enrichment for immune cell associations, pathways, biologic processes, and mouse phenotype. Network visualization of the enriched terms (P = 0.05; false discovery rate correction) was done using the Cytoscape application.[27] A comparison of the genes using specific Gene Ontology (GO) IDs and the gene list was performed.

Multivariable Model for TH

Clinical, demographic, radiologic, and genomic variables were tested for association with baseline LN and future TH using χ^2 tests or nonparametric Wilcoxon tests. Baseline variables were assessed for association with TH with univariate logistic regression analysis with odds ratios (95% confidence intervals [CIs]) calculated for each variable. A multivariable model was developed using iterative testing in a logistic regression for TH. Variables with univariate significance ($P < 0.1$) were considered for inclusion and added sequentially to the final model to maximize the likelihood ratio and optimize model fit criteria based on decreasing Akaike's Information Criteria (AIC). To assess for model overfitting, the McFadden's R^2 and adjusted R^2 values were calculated as each variable was added, with increasing values showing appropriate model fitting. Logistic regression analysis and receiver operating characteristic curves were generated with SAS v.4 (SAS Institute, Cary, NC).

Ethical Considerations

Each site reviewed and approved the protocol and appropriate written informed consent with their institutional review board. Consent was obtained in all cases from patients or parents/guardians. All participants provided assent as appropriate.

RESULTS

RISK Cohort and Subgroup Clinical Characteristics

As noted, the RISK multicenter study enrolled 1136 children with CD at diagnosis at 28 locations in the United States and Canada. From within this cohort, subgroups were established based on available data for each analysis. Clinical, demographic, and baseline characteristics for the total cohort and each subanalysis group are summarized in Table 1. The subgroups for each analysis were similar to the overall cohort.

Association of Baseline LN With Subsequent TH

Follow-up imaging was available for central reading in 140 patients at a median of 37 months after diagnosis. In the subcohort of patients who had both baseline and follow-up imaging, baseline LN was detected in 51% (41 of 81) of patients. In the subcohort of patients with follow-up imaging used in univariate analysis for TH, the follow-up imaging as defined by Montreal classification showed that 37 (26%) patients had normal follow-up imaging, 11 (8%) had a stricturing disease, 9 (6%) had penetrating disease, and 3 (2%) had stricture-penetrating disease on follow-up imaging. Medication exposures (including prednisone, mesalamine, immune modulators, and anti-TNF therapy) did not vary between patients who achieved TH vs those who did not (Supplemental Table 2). Univariate analysis linked TH with

Table 1. Clinical and Demographic Characteristics of Overall RISK Cohort and Analysis Subgroups

	Overall RISK Cohort	Univariate Analysis for TH on Follow-Up Imaging	TH Multivariable Model	Microbiome vs Baseline Imaging Analysis	Microbiome vs Gene Expression Analysis	Gene Expression vs Baseline Imaging Analysis
	N = 1136	n = 140	n = 84	n = 48	n = 155	n = 40
Demographics						
Age at diagnosis (y)	12.5 (10-14.8)	11.9 (9.9-13.8)	11.6 (9.9-13.8)	13 (10.8-15)	12 (10-14)	11.6 (10.6-14.4)
Male (%)	687 (61)	88 (63)	54 (64)	29 (60)	90 (58)	26 (65)
White race (%)	871 (77)	105 (75)	67 (80)	40 (83)	128 (83)	29 (73)
BMI *Z*-score	–0.6 (–1.6 to 0.2)	–0.7 (–1.6 to 0.3)	–0.5 (–1.6 to 0.5)	–1.1 (–1.8 to –0.2)	–0.6 (–1.6 to 0.3)	–0.7 (–1.8 to –0.2)
Duration of follow-up (mo)	69 (45-92)	82 (67-95)	80 (66-95)	78 (64-95)	70 (52-95)	76 (63-95)
Serologic reactivity at diagnosis						
Albumin (g/dL)	3.6 (3.1-4)	3.4 (3-3.9)	3.4 (2.9-3.8)	3.3 (3-3.9)	3.5 (3.1-3.9)	3.4 (3-3.9)
ASCA IgG (EU/mL)	14.7 (5-38.2)	16.2 (4.6-44.1)	19.8 (4.5-41)	13.7 (4.5-40.9)	16.4 (6.3-37.4)	16 (5.3-41.1)
Baseline disease location by endoscopy	1049	110	78	45	153	35
Isolated terminal ileum	158 (15)	26 (19)	16 (19)	16 (36)	35 (23)	10 (28)
Isolated colonic	298 (28)	31 (22)	23 (27)*	5 (11)	32 (21)	8 (23)
Ileocolonic	593 (57)	63 (45)	39 (46)	24 (53)	86 (56)	17 (49)
Baseline ileal imaging characteristics		99	84	48	18	40
Normal (1)	—	15 (11)	12 (14)	6 (12)	3 (17)	6 (15)
Inflammation only (2)	—	30 (21)	25 (30)	18 (38)	5 (28)	15 (38)
LN (3)	—	48 (34)	43 (51)	21 (44)	9 (50)	17 (43)
Stricture (4)	—	6 (4)	4 (5)	3 (6)	1 (5)	2 (5)
Follow-up imaging characteristics		140	84	17	15	25
Time to follow-up MRE (mo)	—	36.8 (20.8-51.8)	36.6 (18.6-50.1)	21.8 (14.7-49)	29.6 (20.1-54.6)	28.9 (19.6-48.9)
Follow-up TH	—	37 (26)	21 (25)	2 (12)	5 (33)	6 (24)

Data are provided as median (IQR) or n (%) for the overall RISK cohort with inflammatory behavior at diagnosis and the RISK subgroups used for analysis. Baseline ileal imaging characteristics included 4 grades of ileal CD involvement: (1) normal; (2) inflammation-only with wall thickening and hyperenhancement; (3) LN with wall thickening, hyperenhancement, and reduction in the ileal lumen to <50% of the upstream bowel lumen; and (4) stricture, defined as persistent LN with ≥3 cm prestenotic bowel dilation. Parameters with missing data are reported as frequency of total with available data.
*Subsequently, 14 patients had inflammation at baseline imaging by central interpretation.
BMI indicates body mass index; MRE, magnetic resonance enterography.

a higher baseline body mass index *Z* score, higher serum albumin, colon-only disease location defined by baseline ileal colonoscopy, absence of endoscopically identified ileal deep ulcers, lower ASCA serologies, and lower baseline imaging score (range, 1-4) per the AGA-SAR guidelines[7] for ileal CD (Fig. 1 and Supplemental Table 3). Age, sex, and race were not associated with TH. When we evaluated antimicrobial serologies, there was no difference in ASCA serology between patients with and without LN (12.2 EU/mL [7.2-16.8] vs. 11.6 EU/mL [7.6-19], respectively) Median (IQR). Anti-CBir 1 was not associated with TH by univariate analysis, nor was a difference observed in the presence of LN (18.3 EU/mL [11-63.5]) vs no LN (20.3 EU/mL [11.1-48.5]) Median (IQR).

A multivariable logistic regression model was built sequentially with baseline ileal disease location by colonoscopy, ASCA IgG, albumin, and baseline ileal imaging score (Fig. 2 and Table 2). In the final model, the addition of the baseline imaging score resulted in excellent rank-order discrimination for TH with an area under the curve of 86% (95% CI, 77%-95%). Model comparison showed that the AIC decreased from AIC = 109 to AIC = 73 and that the likelihood ratio (LR) test was statistically significant at $P = 0.004$ in the final model. The final model test characteristics included the following: accuracy, 86% (95% CI, 76%-92%); sensitivity, 57% (95% CI, 34%-78%); specificity, 95% (95% CI, 87%-99%); positive predictive value, 80% (95% CI, 56%-93%); negative predictive value, 87% (95% CI, 80%-92%); positive likelihood ratio, 12 (95% CI, 4-38); and negative likelihood ratio, 0.5 (95% CI, 0.3-0.7; Table 2). Collectively, these data showed that pediatric patiets with CD with ileal location,

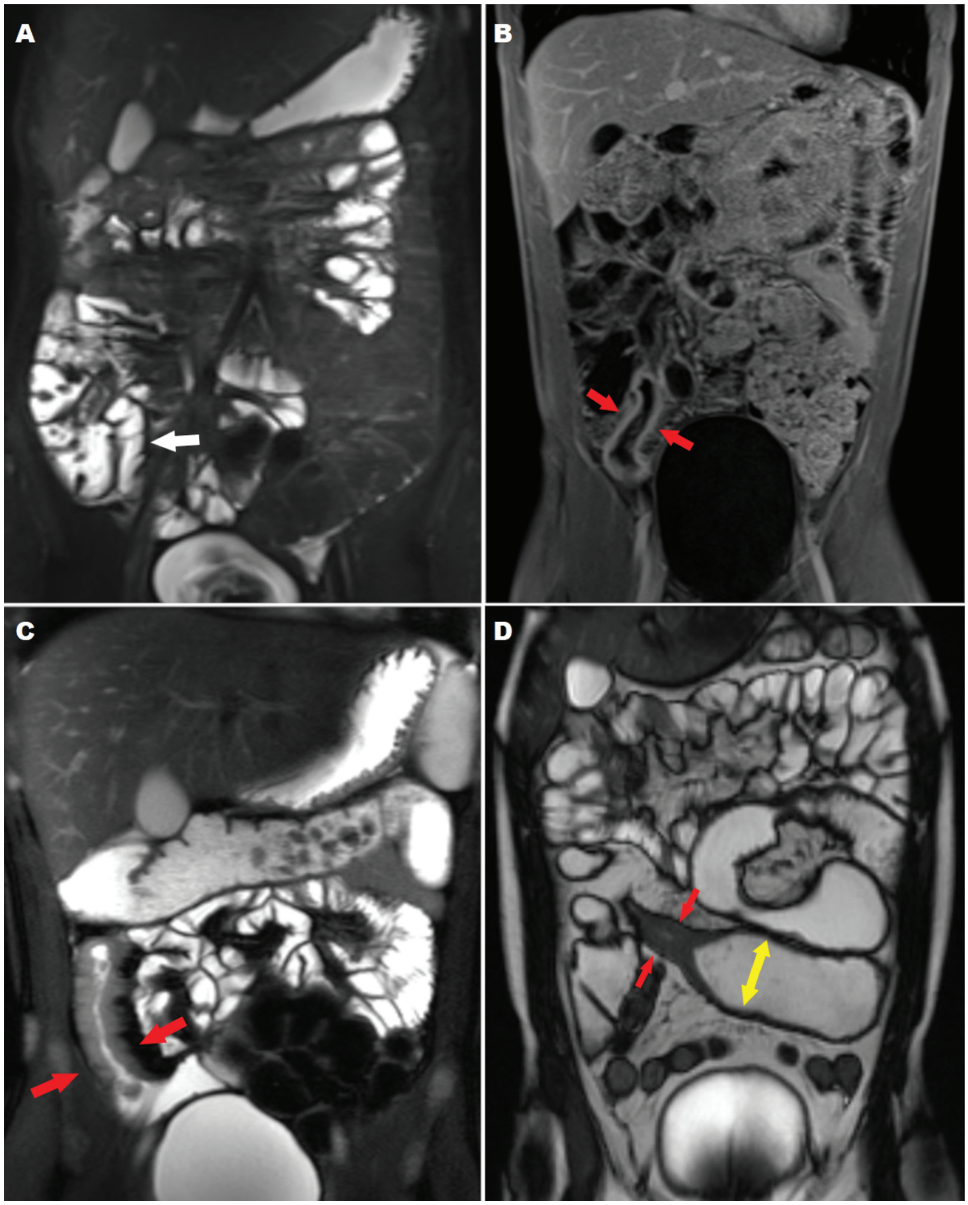

Figure 1. Classification of baseline ileal imaging appearances. Imaging classification of ileal CD progression was performed using AGA-SAR consensus guidelines.[7] Representative coronal images for each of the 4 categories are shown. A, Normal TI without wall thickening (white arrow), mural edema, or LN (coronal view, single-shot fast spin-echo sequence). B, Active inflammation only of TI with mild wall thickening and postcontrast hyperenhancement (red arrows) along with adjacent mesenteric vascular engorgement, consistent with B1 inflammatory disease without LN (coronal view, contrast-enhanced T1-weighted sequence). C, LN with active inflammation (wall thickening and intramural edema) of TI (red arrows) without overt upstream dilation. The TI lumen was reduced to <50% of the more proximal small-bowel lumen. The more proximal small bowel-lumen measured <3 cm (coronal view, single-shot fast spin-echo sequence). D, Strictured TI with wall thickening and LN as denoted by red arrows. The prestenotic bowel lumen was dilated and measured ≥3 cm (yellow arrows; coronal view, steady-state free precession sequence). TI indicates terminal ileum.

LN, low albumin, and increased ASCA IgG were less likely to achieve TH (Table 2).

Elevation of Profibrotic Ileal Gene Signatures in the Presence of LN

Based on the significance of baseline LN in the predictive multivariable model, we considered analyzing the differential gene expression in patients with LN compared with those without LN. In the DESeq analysis, we found an upregulation of 393 genes and a downregulation of 736 genes for patients with baseline LN (Supplemental Table 4). Gene-set enrichment analyses of the downregulated genes included oxidoreductase and transporter activity (P = 3.6E-10 and 1.4E-8, respectively), carboxylic acid metabolic processing (P = 1.6E-31), and a novel association with lipid metabolic processing (P = 4.4E-29; Table 3). Enriched cellular components were related to brush border (P = 4.7E-22) and microvillus (P = 2.7E-20) architecture and emphasized genes expressed by ileal enterocytes (P = 3.1E-68). Consistent with this finding, pathways including retinol metabolism (P = 1.7E-8), arginine and proline metabolism (P = 3.5E-6), and peroxisome proliferator-activated receptor (PPAR) signaling (P = 3.6E-6) were predicted to be suppressed in patients with CD with baseline ileal LN. Enrichment of the upregulated

gene signatures revealed enhanced cytokine (P = 1.3E-4) and extracellular matrix production (P = 3.2E-4), cell adhesion (P = 4.7E-4), metal ion homeostasis (P = 2.5E-4), and B-cell receptor signaling (P = 2.6E-2). Consistent with this finding, data emphasized an enrichment of B cells (P = 5.2E-18) and activated fibroblasts (P = 1.8E-15) in the ileum of patients with LN.

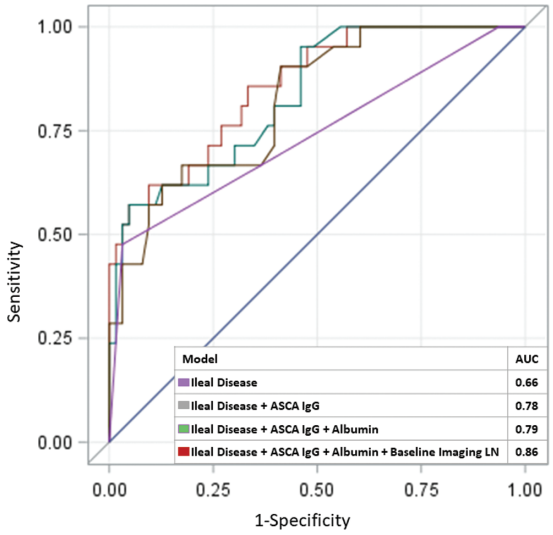

Figure 2. ROC curves for multivariable models for small-bowel TH at follow-up. A subgroup from the RISK study[6] (n = 84) with complete data for disease location, serum ASCA IgG, serum albumin, and baseline ileal imaging grade was used to derive a multivariable model for normal small-bowel imaging during follow-up. ROC curves shown for model 1 (ileal disease location by colonoscopy, purple), model 2 (ileal disease location + serum ASCA IgG, black), model 3 (ileal disease location + serum ASCA IgG + serum albumin, green), and model 4 (ileal disease location + serum ASCA IgG + serum albumin + baseline ileal imaging grade for LN, red). The AUROC for each model was as shown. AUROC indicates area under the receiver operating characteristic curve; ROC, receiver operating characteristic.

Next, we evaluated whether patients with LN would also exhibit differential expression of gene signatures previously associated with disease complications. Prior studies[6] have indicated mechanisms for fibrosis development linked to gene enrichment for inflammatory (569 genes) and extracellular matrix (69 genes) pathways as being profibrotic, whereas a respiratory electron transport gene signature (179 genes) was identified as protective in patients with CD with respect to stricture complications. Ileal gene expression for the extracellular matrix, inflammatory, and respiratory gene signatures was reduced to principal components analysis PC1 (Fig. 3A), and we were able to show that patients with LN showed similar differences regarding these pathways. Patients with CD with LN exhibited increased inflammatory and extracellular matrix PC1 and reduced respiratory PC1, compared with patients without LN.

To capture how the inflammatory, extracellular matrix, and respiratory pathways connected with each other and with other pathways, we built a common network analysis. The extracellular matrix and inflammatory networks were notable for signaling through platelet-derived growth factor and the PI3K-Akt pathway and for expression by CD ileal fibroblasts and inflammatory macrophages, respectively (Fig. 3B). The inflammatory signature was also linked to cellular apoptosis, TNF signaling, and integrin pathways. Conversely, the respiratory signature was primarily associated with mitochondrial function such as pyruvate metabolism expressed by enterocyte progenitors.

Association of LN With Shifts in Ileal Microbial Communities

Subsequently, we tested for a direct association between baseline LN and changes in microbial communities. Neither overall ileal microbial alpha- nor beta-diversity varied with the presence of LN (Supplemental Fig. 2). We did observe a decrease in ileal microbial alpha-diversity as the age at diagnosis increased from 6 to 16 years of age (P = 0.03; Supplemental Fig. 3). No differences in alpha- or beta-diversity were observed based on sex or race.

Table 2. Multivariable Models for Small Bowel TH at Follow-Up

	Model 1		Model 2		Model 3		Model 4	
	OR (95% CI)	*P*	OR (95% CI)	*P*	OR (95% CI)	*P*	OR (95% CI)	*P*
Baseline predictor								
Ileal location by colonoscopy	0.2 (0.07-0.56)	0.002	0.16 (0.05-0.49)	0.0014	0.14 (0.04-0.44)	0.001	0.2 (0.05-0.87)	0.03
ASCA IgG (EU/mL)	—	—	0.97 (0.94-0.99)	0.011	0.97 (0.94-0.99)	0.013	0.97 (0.95-1)	0.06
Albumin (g/dL)	—	—	—	—	2.5 (1-6.5)	0.056	4 (1.3-12.3)	0.016
Baseline ileal imaging characteristics (1,2,3,4)	—	—	—	—	—ww	—	0.3 (0.1-0.8)	0.012
Model comparison								
AUC	0.66 (0.55-0.76)		0.78 (0.67-0.89)		0.79 (0.69-0.90)		0.86 (0.77-0.95)	
AIC	108.56		91.52		86.34		72.7	
McFadden's R^2	0.09		0.2		0.23		0.32	
Adjusted R^2	0.08		0.18		0.2		0.28	
Likelihood ratio test (*P* value)	—		0.001		0.07		0.004	

Baseline predictors are shown with odds ratios with 95% CI in parentheses. Model performance was assessed using the AUC and the AIC, with the goodness-of-fit of successive models tested using the likelihood-ratio test. Baseline ileal imaging characteristics included 4 grades of ileal CD involvement: (1) normal; (2) inflammation-only with wall thickening and hyperenhancement; (3) LN with wall thickening, hyperenhancement, and reduction in the ileal lumen to <50% of the upstream bowel lumen; and (4) stricture defined as persistent LN with ≥3 cm prestenotic bowel dilation.
AIC indicates Akaike's Information Criteria; AUC, area under the curve; CI, confidence interval; OR, odds ratio.

Table 3. Functional Annotation Enrichment Analysis of Genes Differentially Expressed with Ileal LN

Category	Downregulated Genes in the Presence of LN	FDR B&H	ID
Molecular function	Oxidoreductase activity	3.56E-10	GO:0016491
	Transporter activity	1.41E-08	GO:0005215
Biological process	Carboxylic acid metabolic process	1.58E-31	GO:0019752
	Lipid metabolic process	4.44E-29	GO:0006629
Cellular component	Brush border	4.71E-22	GO:0005903
	Apical plasma membrane	9.92E-21	GO:0016324
	Microvillus	2.73E-20	GO:0005902
Pathway	Biological oxidations	2.27E-13	1270189
	Metabolism of lipids and lipoproteins	2.36E-12	1270001
	Retinol metabolism	1.67E-08	83020
	Arginine and proline metabolism	3.46E-06	M2551
	PPAR signaling pathway	3.59E-06	83042
ToppCell Atlas	AdultJeJunum-Enterocyte|AdultJeJunum/shred by tissue - cell type - sample	6.86E-96	e12ec95f830159946d2c eab6479e2c17cce20b88
	AdultIleum-Enterocyte|AdultIleum/shred by tissue - cell type - sample	3.13E-68	7e1000d2972e2cad523b ab9a9191f527f4843f57
Category	**Upregulated Genes in the Presence of LN**	**FDR B&H**	**ID**
Cellular component	Extracellular matrix	3.15E-04	GO:0031012
	Collagen trimer	3.74E-03	GO:0005581
Biological process	Biological adhesion	4.68E-04	GO:0022610
	Regulation of cytokine production	1.34E-04	GO:0001817
	Metal ion homeostasis	2.48E-04	GO:0055065
Mouse phenotype	Abnormal humoral immune response	4.58E-04	MP:0001800
	Abnormal B cell physiology	1.49E-03	MP:0002459
Pathway	Ensemble of genes encoding extracellular matrix and extracellular matrix-associated proteins	1.79E-07	M5889
	NF-kappa B signaling pathway	1.54E-03	634527
	B-cell receptor signaling pathway	2.56E-02	M5436
ToppCell Atlas	BLOOD—(2) B celll/shred on tissue, inflammation status, cell class (v3), cell subclass (v2)	5.20E-18	d9f2cab7f9e7aa476d9bc f5d15896113e59e03f8
	ILEUM-inflamed-(8) Activated fibroblasts|inflamed/shred on tissue, inflammation status, cell class (v3), cell subclass (v2)†	1.79E-15	317f412996d463ddf2e6 a52ff41d5d676c77f43f

FDR B&H, false discover rate Benjamini and Hochberg.

Next, we tested for associations between baseline LN by imaging and specific microbial taxa. Using moderated binomial regression, direct comparison between baseline LN and microbial composition was evaluated. In models adjusting for age at diagnosis, sex, and race, several taxa were associated with LN (Fig. 4A). This association was notable for increased abundance of gram-negative bacterial genera including Enterobacteriaceae and Bacteriodes in the presence of LN. Conversely, there was a reduction in abundance of commensal butyrate–producing bacterial genera with LN, including Faecalibacterium and Eubacterium.

Finally, we tested for relationships between extracellular matrix, inflammatory, and respiratory gene signatures and variation in microbial abundance (Fig. 4B). Butyrate-producing commensal taxon Lachnospiraceae and the *Roseburia* and *Odoribacter* genera were increased with respiratory gene expression and decreased with inflammatory and extracellular matrix gene expression. *Phascolarctobacterium* was associated with reduced respiratory gene expression, and *Aggregatibacter* and *Blautia* were associated with reduced extracellular matrix gene expression. Collectively, these data showed inverse relationships between ileal microbes and gene signatures that were increased (inflammatory and extracellular matrix signatures) or decreased (respiratory signature) in pediatric patients with CD with LN.

Discussion

Recent studies have suggested that the achievement of TH is associated with better outcomes in CD.[5] However, clinical factors around the time of diagnosis associated with future TH are less well understood. Moreover, whereas gene signatures and potentially microbes were previously associated with developing disease complications during follow-up, it was unclear whether these were also associated with the imaging findings at diagnosis. Here, we used the recently created AGA-SAR consensus guidelines for grading ileal inflammation[7] and important clinical metadata included in a multivariable model for TH. We found that pediatric patients with CD with baseline ileal LN, lower serum albumin, and elevated ASCA IgG serology were less likely to achieve future TH. Baseline LN in turn was associated with a decreased

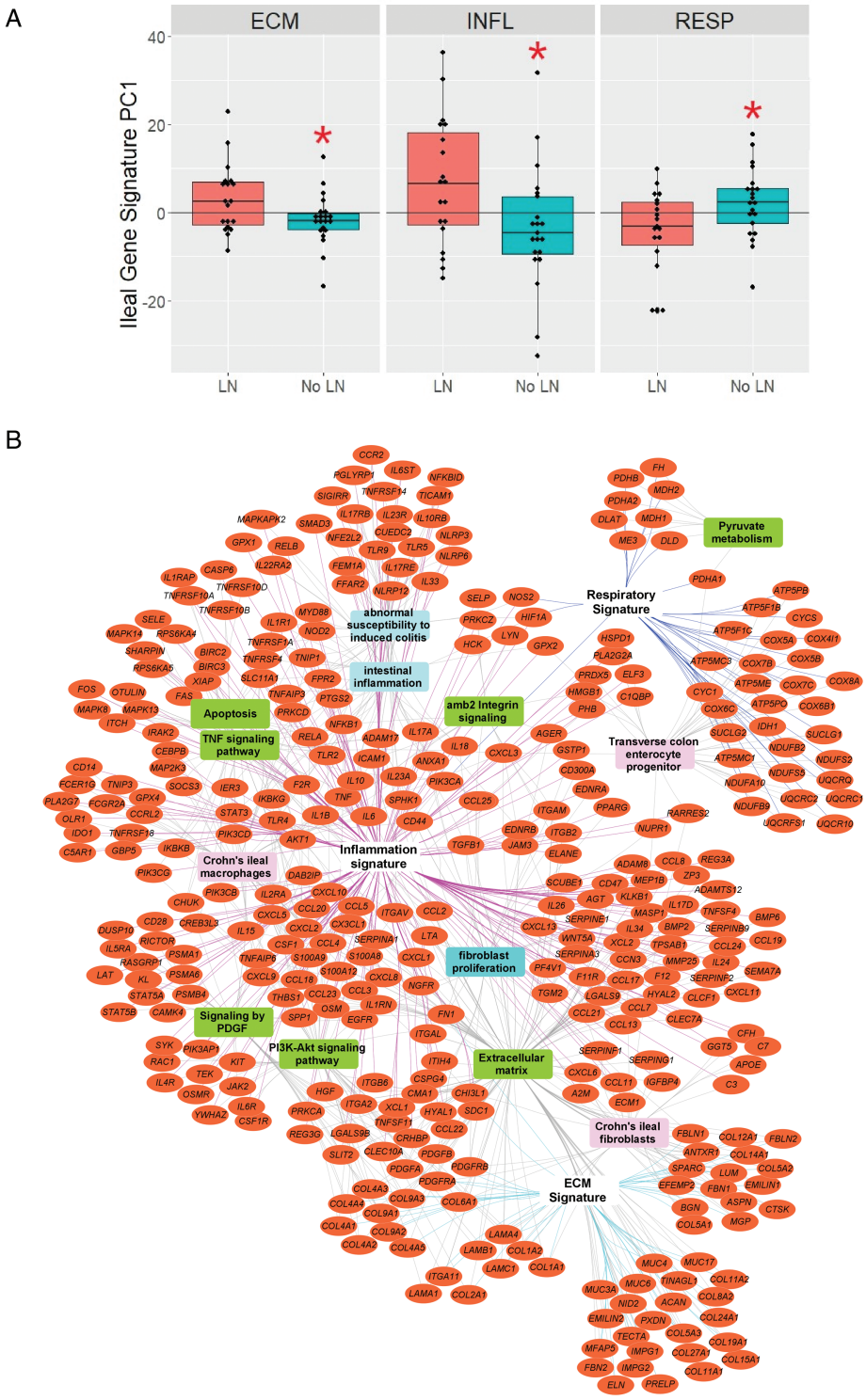

Figure 3. Variation of ileal gene signatures with baseline LN. A, RNA was isolated from pretreatment ileal biopsies and underwent RNA sequencing to define gene expression signatures. Gene expression data were reduced to PC1 for each patient based on predefined gene expression pathways for respiratory electron transport chain (n = 179 genes), inflammatory (n = 569 genes), and extracellular matrix (n = 69 genes) function. Box plots are shown as the median (IQR) and range for extracellular matrix PC1, inflammatory PC1, and respiratory PC1 for patients with and without LN, n = 40, $*P < 0.05$ by *t* test. B, Functional annotation enrichment analyses of extracellular matrix, inflammatory, and respiratory gene signatures were performed using ToppGene Suite and ToppCluster. The enrichment network was generated using Cytoscape. Red ellipses in the network represent genes from each of the 3 signatures (extracellular matrix, inflammatory, and respiratory genes). Rectangle nodes represent enriched terms or features; green rectangles represent pathways, blue and turquoise rectangles represent mouse phenotypes and biological processes (respectively), and pink rectangles represent enriched cell types. Pink, navy blue, and sky-blue ines represent gene associations with the inflammatory, respiratory, and extracellular matrix gene signatures, respectively. IQR indicates interquartile ratio. ECM, extracellular matrix; INFL, inflammatory; RESP, respiratory.

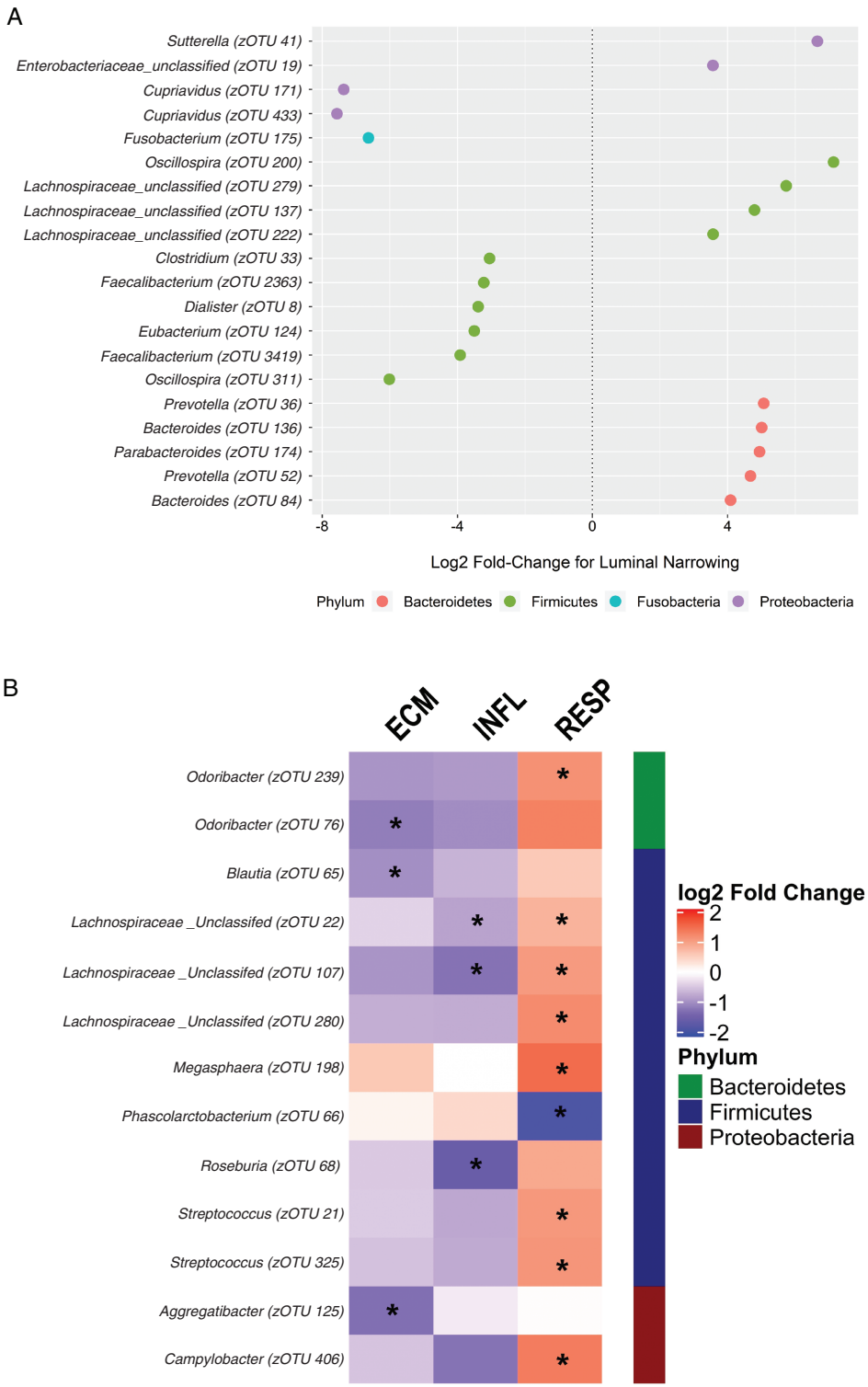

Figure 4. Variation in ileal microbial relative abundance with baseline LN and host gene expression signatures. A, DNA isolated from pretreatment ileal biopsies. Microbe relative abundance determined by 16S rRNA sequencing. Ileal LN determined using baseline imaging grading of ileal CD progression as per AGA consensus guidelines. Log2-fold changes for zOTUs associated with LN as estimated from moderated negative binomial regression (n = 48). zOTUs with FDR *P* values < 0.1 shown after adjustment for age, sex, and ethnicity. B, RNA and DNA isolated from pretreatment ileal biopsies (n = 155). Host gene expression determined using RNA sequencing. Microbial relative abundance determined using 16S rRNA sequencing. Heatmap of log2 fold-changes for zOTUs associated with ECM, INFL, and RESP gene signature PCs as estimated from moderated negative binomial regression. zOTU with FDR *P* values < 0.1 shown. Blue and red indicate negative and positive associations, respectively. ECM indicates extracellular matrix; FDR, false discovery rate; INFL, inflammatory; PC, principal component; RESP, respiratory.

abundance of ileal commensal microbial communities and host metabolic pathways and an increase in pathobionts and proinflammatory and profibrotic gene expression. This work highlights the significance of baseline LN through its association with changes in gene expression and microbial communities and as a predictor of decreased odds for future TH.

The use of these new AGA-SAR consensus guidelines for staging small-bowel CD has improved the identification of LN as early evidence of impending stricturing disease, which likely at least in part reflects smooth muscle hyperplasia.[7] In resected surgical samples from patients with strictures, the smooth muscle hyperplasia/hypertrophy of the muscularis mucosa layer was positively correlated with strictures by imaging, specifically measuring the correlation between prestenotic bowel dilation ≥3 cm and stricture formation.[28-30] Stidham et al[31] were able to show a semi-automated analysis technique with good agreement between trained radiologists for quantitatively assessing LN based on the AGA-SAR scoring system. In a recent study, baseline MRE features of severe ileal disease and creeping fat were predictive of anti-TNF response; however, no distinction was provided between LN and overt stricture.[32] Future studies should ideally incorporate automation methods to better define the spectrum of inflammation, smooth muscle hyperplasia, and increased collagen content represented by ileal LN.

Ileal fibrosis can be mediated by both inflammatory and noninflammatory pathways, as suggested by outcomes with current anti-inflammatory biologic therapies.[33] To evaluate these pathways, we then transitioned in this study to evaluate previously identified gene signatures that were associated with future stricturing behavior.[13] Two different approaches were utilized to test for genes that are linked with baseline LN: direct differential expression (between LN vs no LN) and testing of the previous reported signatures linked with future stricturing.[6] These 2 approaches overall found a downregulation of certain metabolic processes that partially overlapped with the previously defined respiratory gene signature. A similar analysis for the upregulation of genes was associated with genes in the extracellular matrix and inflammatory pathways. Whereas the extracellular matrix and inflammatory principal components (PCs) were significantly enhanced in the presence of baseline LN, there was a decrease in the respiratory PC. Recent single-cell analysis[34] of adult CD ileal resection specimens identified a gene signature for inflammatory macrophages and fibroblasts in a subset of patients. Using the ToppCell Atlas,[25],[26] we found that the inflammatory and extracellular matrix gene signatures detected in ileal mucosal biopsies associated with LN in the current study included genes expressed by inflammatory macrophages and fibroblasts detected using single-cell analysis of adult CD surgical specimens.[34] Respiratory signatures are likely expressed by epithelial and immune cells, and the extracellular matrix signatures are expressed by stromal cells.[34] Remarkably, these gene expression patterns were in turn associated with microbial shifts including the loss of beneficial commensals and increases in the microbes known to drive inflammation. The use of mucosal biopsy samples can begin to elucidate the drivers of TH, but research using surgical specimens and single-cell methodologies will be important to evaluate cell types and pathways that may contribute to transmural disease.

Finally, we asked whether microbial shifts would also be associated with LN and these host gene signatures. An association between the enhancement of potential pathobionts and the suppression of commensal microbes with a history of surgery was recently reported; these included differential abundances of *Enterobacter* and *Fusobacterium*.[35] A similar pattern was observed in this study with decreased *Faecalibacterium* and *Eubacterium* in patients with LN. *Dialster* has been associated with a diet high in wheat-barley-rice, which can reduce interleukin-6-driven inflammation[36] and was observed in patients without LN in this study. The 3 genera of the Lachnospiraceae taxon that were more abundant in the presence of LN could represent the identification of genus-level bacteria such as *Ruminococcus gnavis,* which can be classified within this genus. This possibility may explain the present association with LN because *R. gnavis* is more commonly associated with increased IBD disease activity.[37] *Fusobacterium* is usually associated with high oxidative stress and would be expected to be present in inflamed mucosa.[38] However, we observed a greater abundance in patients without LN, which may represent a unique strain of *Fusobacterium* that thrives in a healthier environment compared to a typical environment.

Sutterella is a gram-negative, primarily anaerobic bacterial that has been highly negatively correlated to achieving steroid-free remission at follow-up in ulcerative colitis in the PROTECT study.[39] A murine model observed an enrichment of *Sutterella* that was more rapidly degrading IgA, leading to reduced mucosal immune function, a possible cause of inflammation in ulcerative colitis.[40] Our study found that *Sutterella* had an increased relative abundance in the presence of LN. Antimicrobial seropositivity, with CBir1 and ASCA, has been associated with stricturing and penetrating behavior,[6] but it has not previously been evaluated for associations with TH. We found that only lower ASCA was associated with TH and that neither antimicrobial serology was associated with baseline LN. Although these results require confirmation in a larger cohort, collectively they suggest the potential for microbial-targeted therapies in patients with LN.

The strengths of this study include the use of the large-multicenter RISK cohort study and new central interpretations of diagnostic imaging analyzed using the newly devised AGA-SAR consensus guidelines for reporting small-bowel CD[7]. Patients' initial disease classification was based on both baseline ileal colonoscopy and imaging; however, many patients did not have baseline imaging at the time of colonoscopy, so we observed a higher portion of patients with colon-only inflammation. Subsequent imaging showed that a large portion of patients in fact had ileal inflammation by imaging, so we elected to include patients with colon-only inflammation. Although there was good agreement for consensus reads for the radiologic images to date, additional validation is necessary. Microbial shifts and differences in gene expression were defined in the pretreatment ileum at the time of diagnosis and so were not confounded by treatment or disease duration. Treatment was dictated by each patient's primary physician and thus was not controlled in the RISK study. Future studies should include standardized therapy based on prospective drug monitoring for biologic therapies and baseline imaging.

One limitation is that the subgroup analysis had smaller numbers of patients because of incomplete data availability for microbial data and gene expression signatures. Follow-up imaging, although limited in subgroup analysis, was critical to evaluate new associations with gene expression signatures and microbial data. Regular follow-up imaging will

be critical in future studies to investigate these associations and correlate with disease progression. In this regard, there were not sufficient participants with complete data for baseline gene expression and microbial abundance, and central reads of both baseline and follow-up MRE, to test our prior reports of inflammatory and extracellular matrix gene expression signatures[6, 13] or microbes[6] associated with future stricturing or internal penetrating disease complications. In addition, future research should include prospectively obtained metagenomic data to determine species-level differentiation of the microbial taxa with the inclusion of a validation cohort with standardized imaging to show the strength of the findings again.

Conclusions

Baseline imaging features, and serum albumin and antimicrobial serology, may be used to estimate the likelihood of future TH in patients with CD. We found that LN is associated with a lower likelihood of healing, specific microbial shifts, and host metabolic and wound healing gene programs. If confirmed in larger cohorts, these data may guide novel microbial-targeted therapies to improved rates of TH in CD.

SUPPLEMENTAL DATA

Supplemental data are available at *Inflammatory Bowel Diseases* online.

Supplemental Table 1. Gene Expression Signatures for Extracellular Matrix, Inflammatory, and Respiratory Gene Signatures

Supplemental Table 2. Maximal Medical Therapy for Patients in Multivariable Model for TH at Follow-Up

Supplemental Table 3. Univariate Analysis for Small Bowel TH at Follow-Up

Supplemental Table 4. DESeq Analysis for Upregulated and Downregulated Genes in Patients With LN

Supplemental Figure 1. Consort diagram for analysis. The RISK Study enrolled 1136 patients with CD at diagnosis. Endoscopically obtained terminal ileum tissue biopsies were obtained at diagnosis for 16S microbial analysis and gene expression analysis. This study performed centralized reading of the radiographic imaging of all available baseline and follow-up imaging. Subcohorts for each analysis were generated based on available data as shown.

Supplemental Figure 2. Microbial alpha- and beta-diversity according to LN. A, Alpha-diversity was tested as observed zOTUs according to LN. B, Shannon diversity according to LN. C, Beta-diversity was tested as principal components analysis ordination according to LN performed on the zOTU count matrix after variance stabling transformation. D, NMDS of the Bray-Curtis similarity according to LN. NMDS indicates nonmetric dimensional scaling; PC2, principal component 2.

Supplemental Figure 3. Microbial alpha- and beta-diversity according to age, sex, and race. A-C, Alpha-diversity was tested as observed zOTUs according to sex, race, and age at diagnosis. D-F, Beta-diversity was tested as principal components analysis ordination according to sex, race, and age at diagnosis performed on the zOTU count matrix after variance stabling transformation. PC2 indicates principal component 2.

Acknowledgments

The results published here are in whole or in part based on data obtained from the IBD Plexus program of the Crohn's & Colitis Foundation. We thank the Crohn's and Colitis Foundation RISK study publication committee and Andres Hurtado-Lorenzo and Gerard Honig of the foundation for coordinating the gene expression and for critical review of this manuscript. We also thank Erin Bonkowski and Elizabeth Maier for technical support and Kajari Mondal and Jarod Prince for project and data management support.

Supported by: This work was supported by grants from the Crohn's & Colitis Foundation (JD, LAD, and SK), the Gene Analysis and Integrative Morphology cores of the National Institutes of Health (NIH)-supported Cincinnati Children's Hospital Research Foundation Digestive Health Center (1P30DK078392-01), NIH grant T32 DK007727 (AT), and NIH grants RO1 DK098231 (LAD and SK) and R01 HD94862 (LAD and NJO).

References

1. Lehtinen P, Ashorn M, Iltanen S, et al. Incidence trends of pediatric inflammatory bowel disease in Finland, 1987–2003, a nationwide study. *Inflamm Bowel Dis*. 2011;17:1778–1783.
2. Benchimol EI, Kaplan GG, Otley AR, et al. Corrigendum: rural and urban residence during early life is associated with a lower risk of inflammatory bowel disease: a population-based inception and birth cohort study. *Am J Gastroenterol*. 2017;112:1485.
3. Rieder F. Managing intestinal fibrosis in patients with inflammatory bowel disease. *Gastroenterol Hepatol (N Y)*. 2018;14:120–122.
4. D'Haens G, Rieder F, Feagan BG, et al. Challenges in the pathophysiology, diagnosis and management of intestinal fibrosis in inflammatory bowel disease. *Gastroenterology*. Published online June 26, 2019. doi: 10.1053/j.gastro.2019.05.072.
5. Chang CW, Wong JM, Tung CC, et al. Intestinal stricture in Crohn's disease. *Intest Res*. 2015;13:19–26.
6. Kugathasan S, Denson LA, Walters TD, et al. Prediction of complicated disease course for children newly diagnosed with Crohn's disease: a multicentre inception cohort study. *Lancet*. 2017;389:1710–1718.
7. Bruining DH, Zimmermann EM, Loftus EV Jr, et al.; Society of Abdominal Radiology Crohn's Disease-Focused Panel. Consensus recommendations for evaluation, interpretation, and utilization of computed tomography and magnetic resonance enterography in patients with small bowel Crohn's disease. *Radiology*. 2018;286:776–799.
8. Castiglione F, Testa A, Rea M, et al. Transmural healing evaluated by bowel sonography in patients with Crohn's disease on maintenance treatment with biologics. *Inflamm Bowel Dis*. 2013;19:1928–1934.
9. Fernandes SR, Rodrigues RV, Bernardo S, et al. Transmural healing is associated with improved long-term outcomes of patients with Crohn's disease. *Inflamm Bowel Dis*. 2017;23:1403–1409.
10. Weinstein-Nakar I, Focht G, Church P, et al.; ImageKids study group. Associations among mucosal and transmural healing and fecal level of calprotectin in children with Crohn's disease. *Clin Gastroenterol Hepatol*. 2018;16:1089–1097.e4.
11. Lloyd-Price J, Arze C, Ananthakrishnan AN, et al.; IBDMDB Investigators. Multi-omics of the gut microbial ecosystem in inflammatory bowel diseases. *Nature*. 2019;569:655–662.
12. Jacob N, Jacobs JP, Kumagai K, et al. Inflammation-independent TL1A-mediated intestinal fibrosis is dependent on the gut microbiome. *Mucosal Immunol*. 2018;11:1466–1476.
13. Haberman Y, Minar P, Karns R, et al. Mucosal inflammatory and wound healing gene programs reveal targets for stricturing be-

havior in pediatric Crohn's disease. *J Crohns Colitis*. Published online August 8, 2020. doi:10.1093/ecco-jcc/jjaa166.
14. Satsangi J, Silverberg MS, Vermeire S, et al. The Montreal classification of inflammatory bowel disease: controversies, consensus, and implications. *Gut*. 2006;55:749–753.
15. Haberman Y, Schirmer M, Dexheimer PJ, et al. Age-of-diagnosis dependent ileal immune intensification and reduced alpha-defensin in older versus younger pediatric Crohn disease patients despite already established dysbiosis. *Mucosal Immunol*. 2019;12:491–502.
16. Dubinsky MC, Kugathasan S, Mei L, et al.; Western Regional Pediatric IBD Research Alliance; Pediatric IBD Collaborative Research Group; Wisconsin Pediatric IBD Alliance. Increased immune reactivity predicts aggressive complicating Crohn's disease in children. *Clin Gastroenterol Hepatol*. 2008;6:1105–1111.
17. Caporaso JG, Lauber CL, Walters WA, et al. Ultra-high-throughput microbial community analysis on the Illumina HiSeq and MiSeq platforms. *Isme J*. 2012;6:1621–1624.
18. Edgar R. UNOISE2: improved error-correction for Illumina 16S and ITS amplicon sequencing. Preprint. Posted online October 15, 2016. bioRxiv. doi: 10.1101/081257.
19. Bolyen E, Rideout JR, Dillon MR, et al. Reproducible, interactive, scalable and extensible microbiome data science using QIIME 2. *Nat Biotechnol*. 2019;37:1091.
20. Janssen S, McDonald D, Gonzalez A, et al. Phylogenetic placement of exact amplicon sequences improves associations with clinical information. *mSystems*. 2018;3. doi: 10.1128/mSystems.00021-18.
21. McMurdie PJ, Holmes S. phyloseq: an R package for reproducible interactive analysis and graphics of microbiome census data. *Plos One*. 2013;8:e61217.
22. Love MI, Huber W, Anders S. Moderated estimation of fold change and dispersion for RNA-seq data with DESeq2. *Genome Biol*. 2014;15:550.
23. Haberman Y, Tickle TL, Dexheimer PJ, et al. Pediatric Crohn disease patients exhibit specific ileal transcriptome and microbiome signature. *J Clin Invest*. 2014;124:3617–3633.
24. Bray NL, Pimentel H, Melsted P, et al. Near-optimal probabilistic RNA-seq quantification. *Nat Biotechnol*. 2016;34:888.
25. Chen J, Bardes EE, Aronow BJ, et al. ToppGene Suite for gene list enrichment analysis and candidate gene prioritization. *Nucleic Acids Res*. 2009;37:W305–W311.
26. Kaimal V, Bardes EE, Tabar SC, et al. ToppCluster: a multiple gene list feature analyzer for comparative enrichment clustering and network-based dissection of biological systems. *Nucleic Acids Res*. 2010;38:W96–W102.
27. Shannon P, Markiel A, Ozier O, et al. Cytoscape: a software environment for integrated models of biomolecular interaction networks. *Genome Res*. 2003;13:2498–2504.
28. Chen W, Lu C, Hirota C, et al. Smooth muscle hyperplasia/hypertrophy is the most prominent histological change in Crohn's fibrostenosing bowel strictures: a semiquantitative analysis by using a novel histological grading scheme. *J Crohns Colitis*. 2017;11:92–104.
29. Zhao S, Dejanovic D, Yao P, et al. Selective deletion of MyD88 signaling in α-SMA positive cells ameliorates experimental intestinal fibrosis via post-transcriptional regulation. *Mucosal Immunol*. 2020;13:665–678.
30. Barkmeier DT, Dillman JR, Al-Hawary M, et al. MR enterography-histology comparison in resected pediatric small bowel Crohn disease strictures: can imaging predict fibrosis? *Pediatr Radiol*. 2016;46:498–507.
31. Stidham RW, Enchakalody B, Waljee AK, et al. Assessing small bowel stricturing and morphology in Crohn's disease using semi-automated image analysis. *Inflamm Bowel Dis*. 2020;26:734–742.
32. Rimola J, Fernàndez-Clotet A, Capozzi N, et al. Pre-treatment magnetic resonance enterography findings predict the response to TNF-alpha inhibitors in Crohn's disease. *Aliment Pharmacol Ther*. 2020;52:1563–1573.
33. Rieder F, Fiocchi C. Mechanisms of tissue remodeling in inflammatory bowel disease. *Dig Dis*. 2013;31:186–193.
34. Martin JC, Chang C, Boschetti G, et al. Single-cell analysis of Crohn's disease lesions identifies a pathogenic cellular module associated with resistance to anti-TNF therapy. *Cell*. 2019;178:1493–1508.e20.
35. Hellmann J, Andersen H, Fei L, et al. Microbial shifts and shorter time to bowel resection surgery associated with C. difficile in pediatric Crohn's disease. *Inflamm Bowel Dis*. 2020;26:1212–1221.
36. Martínez I, Lattimer JM, Hubach KL, et al. Gut microbiome composition is linked to whole grain-induced immunological improvements. *Isme J*. 2013;7:269–280.
37. Hall AB, Yassour M, Sauk J, et al. A novel Ruminococcus gnavus clade enriched in inflammatory bowel disease patients. *Genome Med*. 2017;9:103.
38. Strauss J, Kaplan GG, Beck PL, et al. Invasive potential of gut mucosa-derived Fusobacterium nucleatum positively correlates with IBD status of the host. *Inflamm Bowel Dis*. 2011;17:1971–1978.
39. Hyams JS, Davis S, Mack DR, et al. Factors associated with early outcomes following standardised therapy in children with ulcerative colitis (PROTECT): a multicentre inception cohort study. *Lancet Gastroenterol Hepatol*. 2017;2:855–868.
40. Moon C, Baldridge MT, Wallace MA, et al. Vertically transmitted faecal IgA levels determine extra-chromosomal phenotypic variation. *Nature*. 2015;521:90–93.